Available online at www.sciencedirect.com
ScienceDirect
Journal of Catalysis 249 (2007) 208–219
JOURNAL OF CATALYSIS
www.elsevier.com/locate/jcat

Nanocrystalline cerium oxide produced by supercritical antisolvent precipitation as a support for high-activity gold catalysts

Zi-Rong Tang [a], Jennifer K. Edwards [a], Jonathan K. Bartley [a], Stuart H. Taylor [a], Albert F. Carley [a], Andrew A. Herzing [b], Christopher J. Kiely [b], Graham J. Hutchings [a,*]

[a] *School of Chemistry, Cardiff University, Main Building, Park Place, Cardiff, CF10 3AT, UK*
[b] *Center for Advanced Materials and Nanotechnology, Lehigh University, 5 East Packer Avenue, Bethlehem, PA 18015-3195, USA*

Received 22 January 2007; revised 18 April 2007; accepted 20 April 2007

Available online 8 June 2007

Abstract

Nanocrystalline CeO_2 was prepared by precipitation of a solution of the acetate using supercritical CO_2 as an antisolvent. It was demonstrated that gold supported on this material is very active for the oxidation of CO at ambient temperature, particularly in comparison with CeO_2 prepared in a conventional manner by thermal decomposition of the acetate. Comparing the catalytic performance for CO oxidation with the most active catalysts in the current literature confirms the high activity of these new materials. They are considerably more active than previous Au/CeO_2 catalysts. The catalyst activity was found to be dependent on the precipitation conditions, which in turn was found to influence the dispersion of gold on the support, as evidenced by detailed microscopy and spectroscopy characterization. The most active fresh catalyst exhibited highly dispersed gold and showed no evidence of the existence of Au nanocrystals using detailed STEM analysis. Following reaction with CO/O_2, subtle microstructural changes were apparent, although the morphology of the nanocrystalline CeO_2 support was unchanged; in particular, the Au, which was previously uniformly dispersed, showed signs of beginning to agglomerate into sub-5 nm particles. The stability and origin of the catalytic activity are discussed.

Keywords: Gold catalysis; Supercritical media; CO oxidation; Cerium oxide

1. Introduction

Oxidation is a key process that can be used to functionalize molecules using selective oxidation or to remove pollutants using total oxidation. Increasing attention is being given to green chemical reactions, which focuses interest on the design of chemical processes that are atom-efficient. This is particularly true in the fine chemicals industry, where many reactions are done with low atom efficiency [1]. Recently, there has been interest in using gold as a catalyst for oxidation by O_2 [2–4]. Gold dispersed on oxide supports exhibits excellent activity in various important catalytic redox reactions, including CO oxidation [5], which is particularly useful for the purification of hydrogen in fuel cells [6,7]. Supported gold catalysts also have been shown to be very active for the epoxidation of propene [8] and the selective oxidation of alcohols [9]. In recent studies, we have shown that gold can epoxidize alkenes under solvent-free conditions [10] and that supported gold-palladium alloy nanoparticles are highly effective for the direct formation of hydrogen peroxide [11] and oxidation of alcohols [12]. The nature of the supporting matrix for the gold and gold-palladium nanoparticles is of great importance [13–18], and nanocrystalline oxide supports (e.g., CeO_2 and Y_2O_3) have been shown to greatly increase the activity of gold catalysts for CO oxidation compared with supports comprising larger crystallites [16,17].

The extensive literature concerning the low-temperature oxidation of CO has recently been reviewed [19]. In the design of active catalysts for the low-temperature oxidation of CO, much emphasis has been placed on the method of catalyst preparation, as well as the nature of the support, and most investigators

* Corresponding author. Fax: +44 29 2087 4059.
E-mail address: hutch@cf.ac.uk (G.J. Hutchings).

0021-9517/$ – see front matter
doi:10.1016/j.jcat.2007.04.016

agree that high-activity catalysts can be observed with α-Fe_2O_3 [20–26] and TiO_2 [27–35]. Until recently, CeO_2 [16,17,36–38] was not favored as a support, although it was used as a support for very active supported gold low-temperature water-gas shift catalysts [39,40], and although CO oxidation can be considered mechanistically related to the water-gas shift reaction, these catalysts operate at significantly higher temperatures. Recent studies by Corma et al. [16] showed that very active catalysts can be achieved using a nanocrystalline form of CeO_2. However, detailed studies have concentrated on TiO_2 and Fe_2O_3 as supports, and it is now well established that the method of preparation is crucial to controlling the activity of the catalyst [32]. In general, impregnation of titania tends to produce large particles (>10 nm) that are inactive for CO oxidation. Consequently, Haruta et al. [5] devised the method of deposition precipitation, in which a preformed support is stirred in a solution of a gold compound, the pH value is varied by the addition of a base, and small gold nanocrystals are deposited on the surface of the support. This method of preparation has been widely adopted.

The recent interest in using CeO_2 as a support for Au for the CO oxidation reaction has prompted us to study the synthesis and properties of nanocrystalline CeO_2 prepared using a different methodology: precipitation using supercritical CO_2 ($scCO_2$) as an antisolvent. The use of $scCO_2$ as an antisolvent for the controlled precipitation of materials from conventional solvents has been widely applied to the production of a range of materials, including polymers, pharmaceutical chemicals, explosives, superconductors, and catalysts [41–46]. When a solution is brought into contact with $scCO_2$, the solvent power of the conventional solvent is reduced, and the solutes precipitate. Furthermore, the diffusivity of $scCO_2$ is about two orders of magnitude larger than that of conventional liquids. This rapid diffusion can produce supersaturation immediately before precipitation, leading to the formation of nanoparticle morphologies not usually accessible by standard catalyst preparation methods. Using this precipitation method, we have successfully prepared vanadium phosphate catalysts that exhibit enhanced activity compared with conventional materials for the selective oxidation of butane to maleic anhydride [46]. We consider using supercritical carbon dioxide as an antisolvent to facilitate precipitation as the basis of a new green preparation method in which the use of nitrates can be eliminated, thereby decreasing the environmental impact of catalyst preparation in the longer term. We now show that nanocrystalline CeO_2 prepared using this precipitation route can be a highly effective support for Au catalysts for the oxidation of carbon monoxide at ambient temperature.

2. Experimental

2.1. Preparation of CeO_2

Chemicals were purchased from Aldrich and used as received. The synthesis of the $scCeO_2$ was performed as described previously [46]. $scCO_2$ was pumped at pressures of 110–150 bar at a flow rate of 7 ml/min, and the entire system was held at a fixed temperature (40 or 60 °C). A solution of $Ce(acac)_3$ in methanol (13.33 mg/ml) was pumped through a fine capillary into the precipitation vessel at a flow rate around 0.1 ml in co-current mode with $scCO_2$. As the solution exited the capillary, the droplet and $scCO_2$ rapidly diffused into each other, causing the solute to precipitate rapidly. The precursor was recovered and calcined at 400 °C for 2 h. The $unCeO_2$ support was obtained by calcining the unprocessed $Ce(acac)_3$ at 400 °C for 2 h.

2.2. Preparation of gold catalysts

Gold was deposited on the supports by a deposition–precipitation procedure. A solution of H_4AuCl_4 (28 mg) was adjusted to pH 10 using 0.2 M NaOH and added into a slurry containing CeO_2 (200 mg) in water (10 ml), then stirred for 20 h. The solid was recovered by filtration, washed, and dried overnight at 100 °C.

2.3. Catalyst testing

Catalysts were tested for CO oxidation using a fixed-bed microreactor (3 mm i.d.), operated at atmospheric pressure. Typically, CO (0.5% in synthetic air) was fed at 22.5 ml/min and passed over the catalyst (15 mg). The temperature was maintained at 25 °C by immersing the bed in a water bath. The products were analyzed using online GC.

2.4. Catalyst characterization

Materials were characterized by powder XRD using an Enraf Nonius PSD120 diffractometer with a Cu$K\alpha$ source operated at 40 keV and 30 mA. Surface areas were determined by nitrogen adsorption at −196 °C using the BET method. Au loadings were determined using a Varian 55B AA spectrometer.

Samples of each catalyst were prepared for TEM characterization by dispersing the powder in ethanol. A drop of the suspension was then placed on a 300-mesh lacey carbon TEM grid and allowed to dry. Bright-field imaging experiments were carried out in a JEOL 2000 FX TEM operating at 200 kV. Annular dark-field (ADF) imaging and X-ray energy dispersive spectroscopy (XEDS) analyses were carried out at 300 kV using a VG HB 603 dedicated STEM fitted with a Nion Inc. spherical aberration corrector and an Oxford Instruments INCA 300 system for XEDS spectrum imaging.

XPS was done using a Kratos Axis Ultra DLD spectrometer using a monochromatic Al$K\alpha$ X-ray source (75 W) and an analyzer pass energy of 160 eV (survey scans) or 40 eV (detailed scans). Samples were mounted using double-sided adhesive tape, and binding energies are referenced to the C(1s) binding energy of adventitious carbon contamination taken to be 284.7 eV.

Table 1
Details of CeO_2 and Au-CeO_2 catalyst precursors and materials used in this study

Sample	Preparation conditions	BET surface area (m^2/g)	[Au] (wt%)
$Ce(acac)_3$	Used as received	4	–
$unCeO_2$	Direct calcination of $Ce(acac)_3$ at 400 °C, 2 h	115	–
$Au/unCeO_2$	Gold added via deposition–precipitation	128	3.7
$scCe(acac)_3$-1	Supercritical antisolvent precipitation (110 bar, 40 °C)	31	–
$scCeO_2$-1	Calcination of $scCe(acac)_3$-1 at 400 °C, 2 h	34	–
$Au/scCeO_2$-1	Gold added via deposition–precipitation	39	3.6
$scCe(acac)_3$-2	Supercritical antisolvent precipitation (150 bar, 40 °C)	25	–
$ScCeO_2$-2	Calcination of $scCe(acac)_3$-2 at 400 °C, 2 h	31	–
$Au/scCeO_2$-2	Gold added via deposition–precipitation	54	3.4
$scCe(acac)_3$-3	Supercritical antisolvent precipitation (110 bar, 60 °C)	10	–
$scCeO_2$-3	Calcination of $scCe(acac)_3$-3 at 400 °C, 2 h	33	–
$Au/scCeO_2$-3	Gold added via deposition–precipitation	45	3.5

3. Results and discussion

3.1. Catalyst performance for the oxidation of carbon monoxide

Samples of CeO_2 were prepared for use as a catalyst support in two ways (Table 1). First, a standard sample, designated $unCeO_2$, was prepared by calcination of $Ce(acac)_3$ at 400 °C for 2 h. Second, three samples were prepared by precipitation of a solution of $Ce(acac)_3$ in methanol with $scCO_2$ as an antisolvent, under different combinations of pressure and temperature (Table 1). These acetate precursors were amorphous according to powder XRD (Fig. 1a), and no structural information could be derived from Raman spectroscopy (see Supplementary material, Fig. S1A); however, IR spectroscopy made it apparent that the $Ce(acac)_3$ had been modified by this process, because most of the fine structure of the IR spectrum of the parent $Ce(acac)_3$ was now absent (see Supplementary material, Fig. S1B). The acetate precursors were calcined at 400 °C for 2 h to give the corresponding oxides. All four samples were found to be crystalline CeO_2 by XRD (Fig. 1b), and Au (ca. 3.5 wt%) was deposited on these supports using a deposition–precipitation method (Fig. 1c). Details of these materials, including BET surface areas and Au loadings, are given in Table 1.

The materials were then used as catalysts for the oxidation of CO as a standard test reaction. The results, shown in Fig. 2, demonstrate that catalysts derived from the antisolvent precipitation procedure can give high catalytic activity compared with $Au/unCeO_2$, prepared using the CeO_2 made by calcination of the cerium acetate used in the supercritical precipitation method, or a standard Au/Fe_2O_3 catalyst provided by the World Gold Council [47]. When tested with a gas flow rate typical of that required for use in respirators (90,000 ml gas/g catalyst/h), the CeO_2-supported materials all gave stable catalytic performance, whereas the standard Au/Fe_2O_3 catalyst deactivated rapidly. Indeed, we had to increase the gas flow rate by almost a factor of 5 (448,000 ml gas/g catalyst/h) to observe a similar rate of deactivation for the CeO_2-supported materials (Fig. 2), which is significantly higher than that required in a respirator application. For the CeO_2 catalysts evaluated in this study, $scCeO_2$-2 gave the highest activity and the order of reactivity for CO oxidation was $scCeO_2$-2 > $scCeO_2$-3 ≈ $scCeO_2$-1 > $unCeO_2$. The activity of these catalysts will be compared with respect to the activity observed in the best CeO_2-supported catalysts reported to date [16] in subsequent section.

3.2. Characterization of catalysts using TEM and XPS

To determine the origin of this effect, we performed detailed transmission electron microscopy (TEM) and X-ray photoelectron spectroscopy (XPS) investigations of the CeO_2 samples. Preliminary investigations of the precursor support revealed that the $scCO_2$ treatment produced fairly smooth (i.e., nonfaceted) spherical particles similar to those reported previously for vanadium phosphate catalysts made using $scCO_2$ [24]. The support that produced the most catalytically active sample ($scCeO_2$-2) consists of disordered, amorphous spheroid structures before calcination (Fig. 3a). On calcination, each sphere crystallizes to form a pseudospherical agglomerate of CeO_2 nanocrystals (Fig. 3b) composed of primary 3- to 8-nm nanocrystals for all three supercritically prepared materials (Table 2), and there is some tendency for neighboring spheres to sinter and form bridging "necks." Also interesting is a notable drop in contrast in the central region of each sphere, which suggests that they may be hollow. This was subsequently confirmed using STEM-ADF imaging and XEDS mapping. The ADF image (Fig. 4a) shows that the contrast change from the perimeter to the center of the sphere is quite large and clearly suggests the presence of a central pore within the spherical agglomerate. Similarly, the XEDS maps of the Ce-L_α and O-K_α (Figs. 4b and 4c) show that far less of the signal for each element is generated from the central region of the particle. A. The HAADF image of a sc-CeO_2 spherical agglomerate presented in Fig. 5 shows numerous randomly oriented faceted CeO_2 nanocrystallites within the agglomerate. The primary CeO_2 nanoparticles have a hollow CeO_2 sphere morphology, most likely due to the increase in density occurring on crystallization from the amorphous precursor to the more efficiently packed (i.e., denser) polycrystalline form in the calcined catalyst. Because the outer diameter of the spheres are approximately the same size both before and after calcination, densification from the outside-in

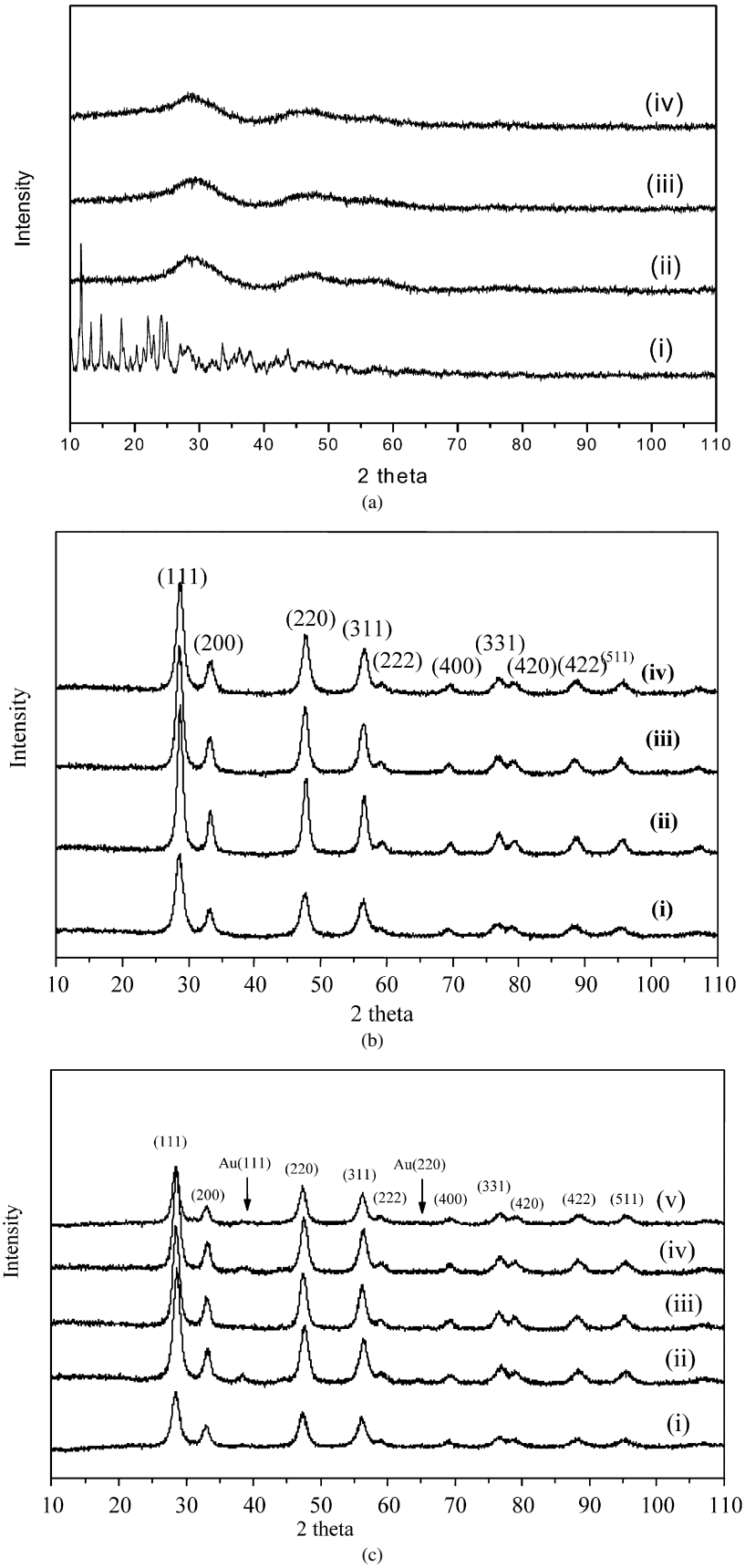

Fig. 1. X-ray diffraction patterns: (a) catalyst precursors—(i) $Ce(acac)_3$, (ii) $scCe(acac)_3$-1, (iii) $scCe(acac)_3$-2, and (iv) $scCe(acac)_3$-3; (b) calcined supports—(i) $unCeO_2$, (ii) $scCeO_2$-1, (iii) $scCeO_2$-2, and (iv) $scCeO_2$-3; (c) the supported Au catalysts—(i) $Au/unCeO_2$, (ii) $Au/scCeO_2$-1, (iii) $Au/scCeO_2$-2, (iv) $Au/scCeO_2$-3, and (v) used-$Au/scCeO_2$-2.

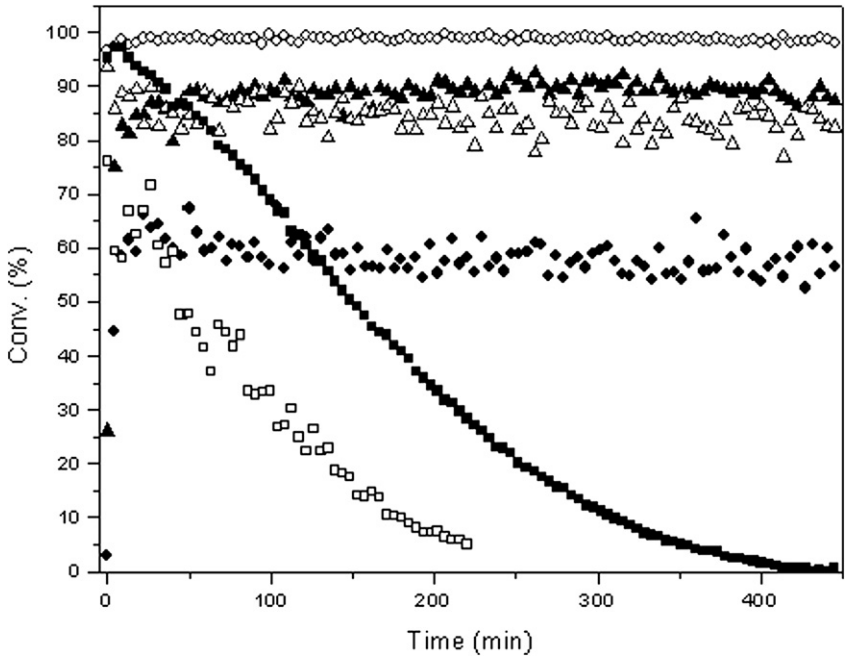

Fig. 2. Catalytic activities for ambient CO oxidation: (●) Au/unCeO$_2$, (△) Au/scCeO$_2$-1, (○) Au/scCeO$_2$-2, (▲) Au/scCeO$_2$-3, (■) 5% wt Au/Fe$_2$O$_3$ (supplied by World Gold Council), and (□) the deactivation of Au/scCeO$_2$-2 using high GHSV (448000 h^{-1}).

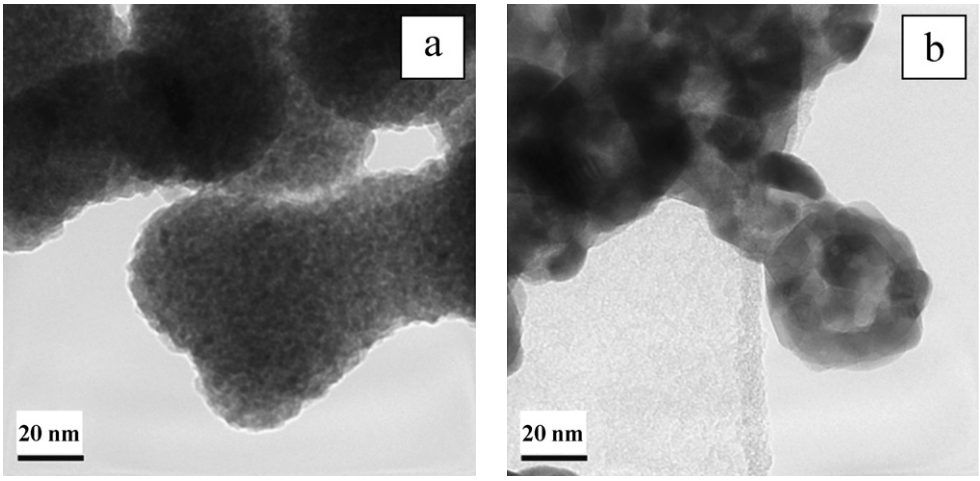

Fig. 3. Bright field TEM micrographs of sample scCeO$_2$-2 showing (a) the amorphous Ce(acac)$_3$ support prior to calcination and (b) polycrystalline CeO$_2$ spheres after calcination at 400 °C.

naturally would result in the formation of a pore within the sphere interior.

Similar morphologies were observed for the other supercritically prepared samples. The major structural difference between the CeO$_2$ support materials treated under differing pressure or temperature was in the size distribution of the polycrystalline spheres after calcination (Table 2). Interestingly, the primary particle size range for unCeO$_2$ was smaller (2–6 nm) than that for scCeO$_2$-1, scCeO$_2$-2, and scCeO$_2$-3 (3–8 nm) (Table 2).

Table 2
Summary of supercritical treatment conditions and resulting CeO$_2$ agglomerate sizes[a]

Sample	Pressure (bar)	Temperature (°C)	Agglomerate size range (nm)	Primary particle size range (nm)
scCeO$_2$-1	110	40	32–75	3–8
scCeO$_2$-2	150	40	45–76	3–8
scCeO$_2$-3	110	60	52–120	3–8

[a] Primary particle size range for unCeO$_2$: 2–6 nm.

Bright-field TEM micrographs of the catalysts after Au deposition and calcination, presented in Fig. 6, show a clear difference in the support morphology between the Au/unCeO$_2$ material (Fig. 6a) and the Au/scCeO$_2$ samples (Figs. 6b–6d). Whereas the scCeO$_2$ samples displayed polycrystalline pseudospherical agglomerates of particles, the unCeO$_2$ sample comprised more irregular and dense agglomerates of faceted crystallites. The gold particles, if present at all, are difficult to discern in such images against the background of the CeO$_2$ crystallites. This is due to the large atomic number of both

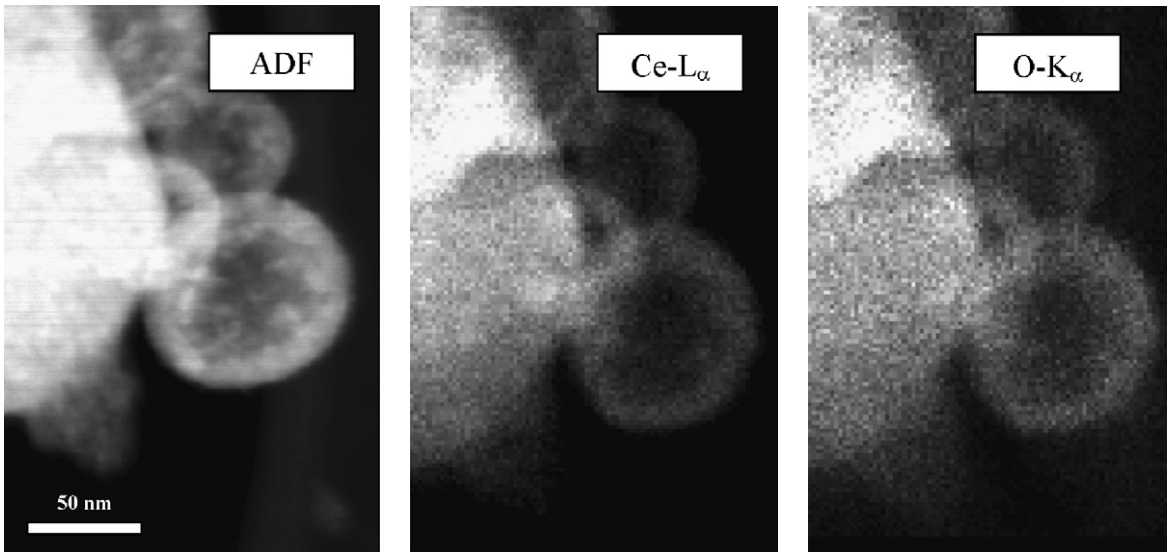

Fig. 4. Montage showing (a) an STEM-ADF micrograph and the corresponding Ce-L_α (b) and O-K_α (c) STEM-XEDS chemical maps of the supercritically treated Au/scCeO_2-2 catalyst.

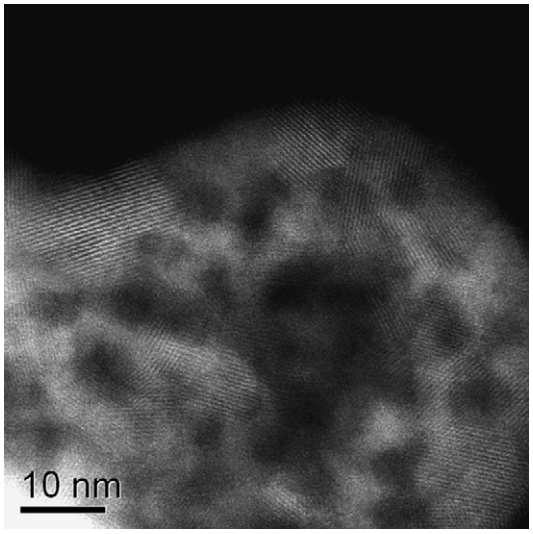

Fig. 5. HAADF image of an sc-CeO_2 spherical agglomerate showing the existence of many individual faceted CeO_2 primary nanocrystallites.

gold and cerium atoms, which leads to similar contrast levels in conventional bright-field TEM images, and the expected similarity in size of the Au particles to the primary CeO_2 crystallites within the agglomerates. For example, the 5-nm crystallites visible on the surface of the arrowed sphere shown in Fig. 6c cannot be conclusively identified as either Au or CeO_2 particles solely on the basis of their relative diffraction contrast or size.

Consequently, it was necessary to use an imaging technique that is more sensitive to atomic number and compositional differences to characterize the gold distribution in these samples. STEM-ADF imaging and STEM-XEDS spectrum imaging are ideal for this task. The Au-M_α X-ray maps, presented in order of increasing catalytic activity (Fig. 7), show the relative dispersion of the Au on the surface of the CeO_2 particles. We attempted to semiquantify the amount of background Au by summing the MSA corrected XEDS spectra from a 5×5 matrix of pixels extracted from the background regions (i.e., away from any particles) from each of the supercritically prepared samples. The count ratio for the Au-L_α:Ce-L_α peaks for the Au-scCeO_2-1, Au-scCeO_2-3, and Au-scCeO_2-2 samples were 0.019, 0.025, and 0.058 respectively. This trend qualitatively indicates a definite progressive increase in the background Au signal in the order Au-scCeO_2-1 $<$ Au-scCeO_2-3 $\ll$ Au-scCeO_2-2. Using the STEM-XEDS spectrum imaging method, it is also possible to get an estimate of the Au particle sizes in these catalysts. Indeed, for the Au-scCeO_2-2 sample, only the background Au signal (i.e., dispersed atoms or sub-1-nm clusters only, which are below resolution of our HAADF imaging and STEM-XEDS) is observed and no larger particles of gold are apparent. For the Au-unCeO_2 sample, no background Au signal is detected, suggesting that the dispersed Au atoms or sub-1-nm clusters are absent, and distinct 10–40 nm particles are observed exclusively. The other two supercritical materials have similarities but differ in the amount of Au background signal and the relative numbers of Au nanoparticles. For Au-scCeO_2-1, a marked number of 2–10 nm particles are visible, coupled with less background Au, whereas for Au-scCeO_2-3, relatively few 2–10 nm particles are visible, coupled with more background Au signal.

The effect of the addition on the BET surface area of the materials on the addition of gold is interesting. An intriguing observation is the increased surface area of the catalysts after impregnation with the gold salt. The typical error limits on these BET measurements is ca. 2–5 $m^2\ g^{-1}$, given the low amounts of material that we have available, and thus these differences are real and reproducible. The effect is due to two contributions. First, a very slight increase in Au-unCeO_2, Au-scCeO_2-1, and

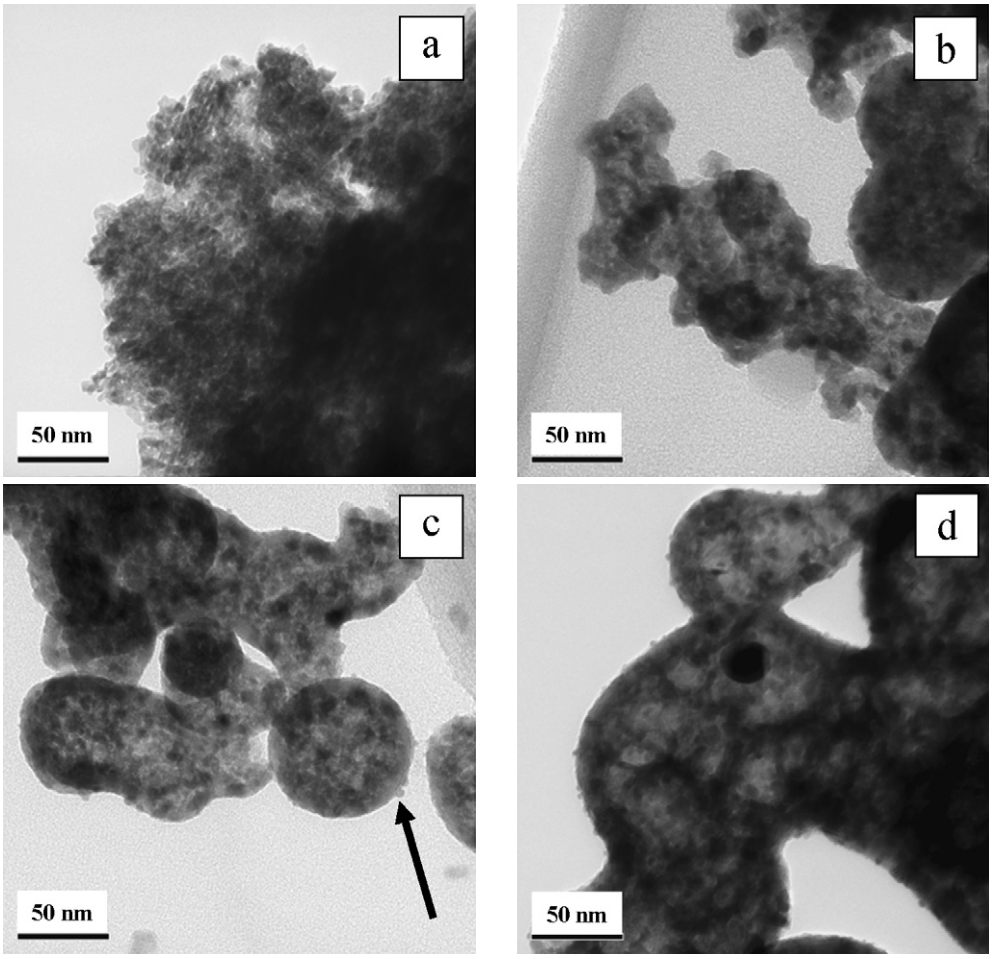

Fig. 6. Representative bright-field TEM micrographs of (a) Au/unCeO$_2$, (b) Au/scCeO$_2$-1, (c) Au/scCeO$_2$-2, and (d) Au/scCeO$_2$-3.

Au-scCeO$_2$-3 is expected due to the additional surface area associated with the Au nanoparticles present in these samples. But on this basis, the Au-scCeO$_2$-2 surface area should look similar to the scCeO$_2$-2 support, because Au nanoparticles are almost absent from this material. We consider the second contribution to the increased surface area to be from partial disruption of the CeO$_2$ agglomerates as the Au is added in a highly acidic aqueous solution.

X-ray photoelectron spectroscopy (XPS) reveals (Fig. 8) that the three catalysts supported on scCeO$_2$ all exhibit an Au(4f) spectrum characteristic of Au^0 with an Au(4f$_{7/2}$) binding energy of 83.7 eV (Figs. 8b–8d). In contrast, for the gold catalyst supported on unCeO$_2$, there are clear signs of two extra components at higher binding energy than the Au^0 peak (Fig. 8a). Scaling spectrum (d) and subtracting it from spectrum (a) generates a difference spectrum that highlights these extra features (Fig. 9). The two components to the difference spectrum have Au(4f$_{7/2}$) binding energies of 84.6 and 85.9 eV, and the relative intensity of the peaks at 83.7, 84.6, and 85.9 eV is 48%:22%:30%. They are likely to arise from the presence of Au(III) and Au(I) species, and we observed an X-ray beam-induced transfer of intensity from the feature at 85.9 eV to that at 84.6 eV (Fig. S2), reflecting the reduction of Au(III) to Au(I) under irradiation with X-rays. An alternative explanation for the two components to the difference spectrum (Fig. 9) in terms of a bimodal particle size distribution (which through final state effects would lead to two different Au(4f) binding energies) is unlikely because of the magnitude of the binding energy shifts of the two components relative to the Au(4f) component for bulk gold; moreover, this interpretation would require the X-ray-induced sintering of Au nanoparticles to explain the spectral changes in Fig. S2, which is not feasible. The high activity of metallic gold nanoclusters in this work contrasts markedly with our previous observations for Au/Fe$_2$O$_3$ catalysts where cationic gold was the active species [11], and highlights the key role of the support. In addition, the presence of cationic gold in the Au/unCeO$_2$ sample also could contribute to the activity of this sample in contrast to the metallic gold-supported catalysts prepared using the supercritical methodology.

The increased dispersion of gold identified in the STEM-XEDS measurements for the supercritically prepared samples compared with the Au/unscCeO$_2$ material, is reflected in the Au(4f):Ce(3d) intensity ratios (Table 3), with the presence of larger particles on the un-sc support leading to a lower intensity ratio. Because XPS measurements provide spatially averaged information, the Au(4f):Ce(3d) intensity ratios, which are affected by the overall particle size distribution and the spread of

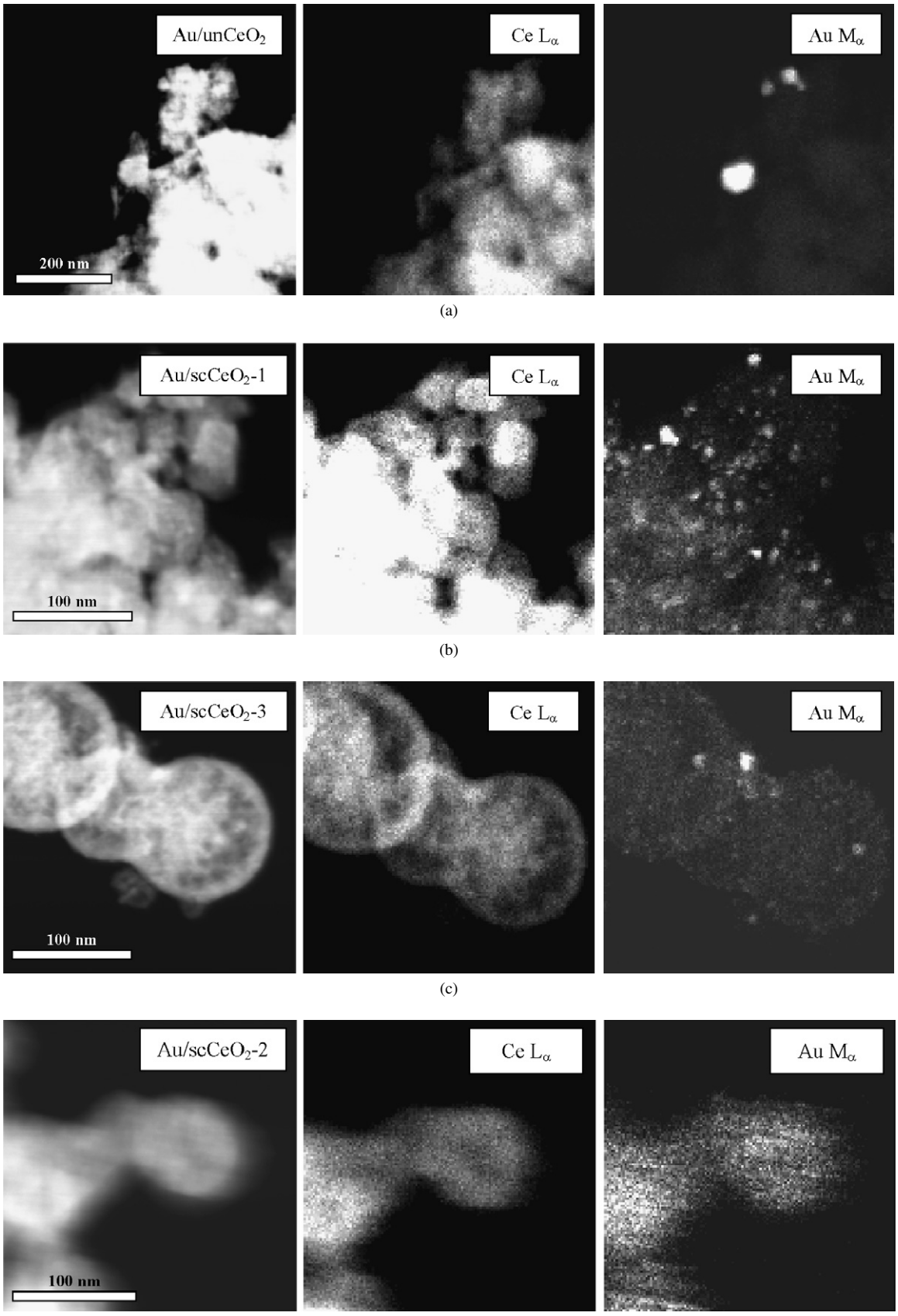

Fig. 7. Montage showing STEM-ADF micrographs *(left column)* and STEM-XEDS spectrum images of Ce-L_α and Au-M_α signals *(center and right columns, respectively)* for Au/unCeO$_2$ (row a), Au/scCeO$_2$-1 (row b), Au/scCeO$_2$-3 (row c), and Au/scCeO$_2$-2 (row d). The catalyst samples are ranked in order of increasing activity for CO oxidation as one travels from the top to the bottom the figure.

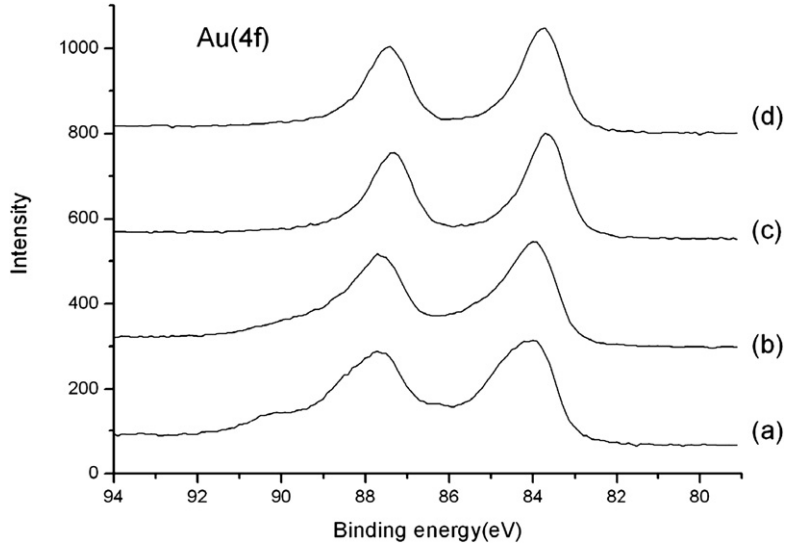

Fig. 8. Au(4f) spectra for the catalysts: (a) Au/unCeO$_2$, (b) Au/scCeO$_2$-1, (c) Au/scCeO$_2$-3, (d) Au/scCeO$_2$-2.

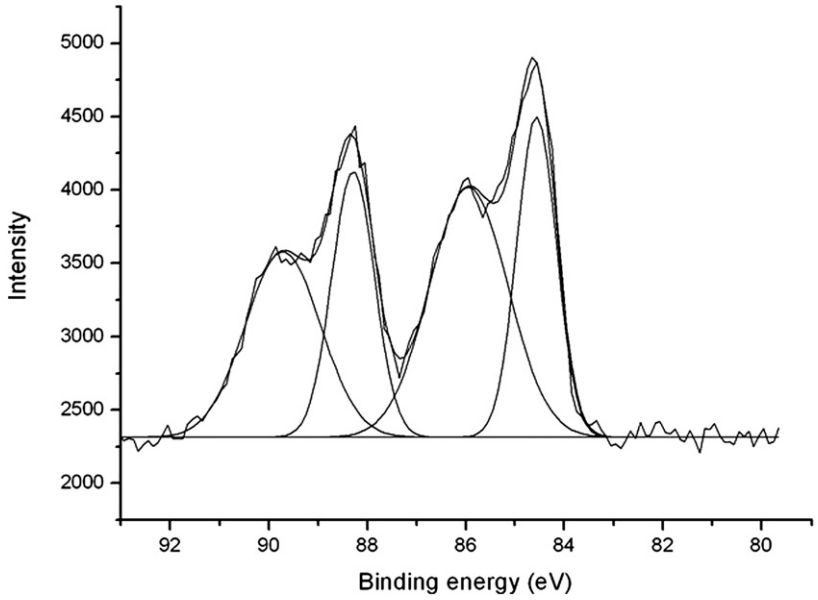

Fig. 9. Au(4f) difference spectrum obtained by subtracting spectrum (d) in Fig. 6 from spectrum (a). The difference spectrum has been curve-fitted to quantify the two species.

values (Table 3), are much lower than would be expected if we considered only extremes of particle size for the samples.

After being used to catalyze the CO oxidation reaction, the Au-scCeO$_2$-2 material was reexamined. The material showed some subtle microstructural changes, as evidenced by the montage of STEM-XEDS maps (Fig. 10). Although the morphology of the nanocrystalline CeO$_2$ support was unchanged, the Au, which was uniformly dispersed earlier, showed signs of beginning to agglomerate into sub-5 nm particles. The Au-L$_\alpha$ map of the used material showed the co-existence of both nanoparticulate and highly dispersed gold, and the XRD pattern (Fig. 1c) was starting to show the presence of crystalline gold. This clearly demonstrates that the deactivation observed is due to agglomeration of the Au.

3.3. Comparison of catalytic performance and comments on the origin of the catalytic activity

As noted earlier, for the CeO$_2$ catalysts evaluated in this study, scCeO$_2$-2 gave the highest activity. The order of reactivity for CO oxidation was scCeO$_2$-2 $>$ scCeO$_2$-3 $\approx$ scCeO$_2$-1 $>$ unCeO$_2$. First, it is important to contrast and compare the activity observed for these four materials with the highest activities reported for Au/CeO$_2$ catalysts [16]. As noted by Corma et al. [16], most early studies using CeO$_2$ as a support for Au catalysts did not result in high activity. In that seminal study of this support material, the authors clearly demonstrated that high-activity catalysts could be obtained when the CeO$_2$ was prepared in a nanocrytalline form. Comparison of the activ-

ities of the catalysts used in the present study and the previous study is not straightforward, because different catalyst evaluation conditions were used (e.g., our contact time was $W/F = 0.05\ g_{cat}\,h\,mol_{CO}^{-1}$, whereas the earlier studies used a much longer contact time of 94 $g_{cat}\,h\,mol_{CO}^{-1}$ [16]). Thus, the space velocities that we used in our studies (as required by catalysts in respirator applications) are 1880 times higher than those used in the previous studies. The 2.8 wt% Au/CeO_2 catalyst [16] exhibited a specific rate of 0.38 $mol_{CO}\,h^{-1}\,g_{cat}^{-1}$ at 5 °C, which was considered comparable with the best reported catalytic data of Haruta et al. [48,49]. At 25 °C, the four catalysts used in this study gave specific rates of Au/scCeO$_2$-2 (3.7 wt% Au) = 19.8 $mol_{CO}\,h^{-1}\,g_{cat}^{-1}$, Au/scCeO$_2$-3 (3.4 wt% Au) = 18.0 $mol_{CO}\,h^{-1}\,g_{cat}^{-1}$, Au/scCeO$_2$-1 (3.7 wt% Au) = 16.9 $mol_{CO}\,h^{-1}\,g_{cat}^{-1}$, and Au/unCeO$_2$ (3.5 wt% Au) = 11.9 $mol_{CO}\,h^{-1}\,g_{cat}^{-1}$. At 5 °C, the specific rate of the most active of these catalysts Au/scCeO$_2$-2 (3.7 wt% Au) was 10.5 $mol_{CO}\,h^{-1}\,g_{cat}^{-1}$ under steady-state conditions, representing a substantial increase over the specific rate observed previously for 2.8 wt% Au/CeO_2 of 0.38 $mol_{CO}\,h^{-1}\,g_{cat}^{-1}$. Indeed, all of the catalysts that we studied had exceptionally high activity compared with previously reported catalysts.

Table 3
XPS derived Au(4f):Ce(3d) intensity ratio for the catalyst samples

Sample	Au(4f)/Ce(3d)[a]
Au/unCeO$_2$	0.101 ± 0.005
Au/scCeO$_2$-1	0.164 ± 0.008
Au/scCeO$_2$-2	0.133 ± 0.007
Au/scCeO$_2$-3	0.134 ± 0.007
Au/scCeO$_2$-2 (used)	0.110 ± 0.005

[a] Au(4f) intensity = Au($4f_{7/2}$) + Au($4f_{5/2}$); Ce(3d) intensity = sum of intensities of the peaks at binding energies of ca. 881 and 870 eV.

Attempting to gain insight into the origin of this enhanced activity is important. We do not consider the enhancement that we observe to be due to the nanocrystalline nature of the primary CeO_2 particles, because in our case they are all very simi-

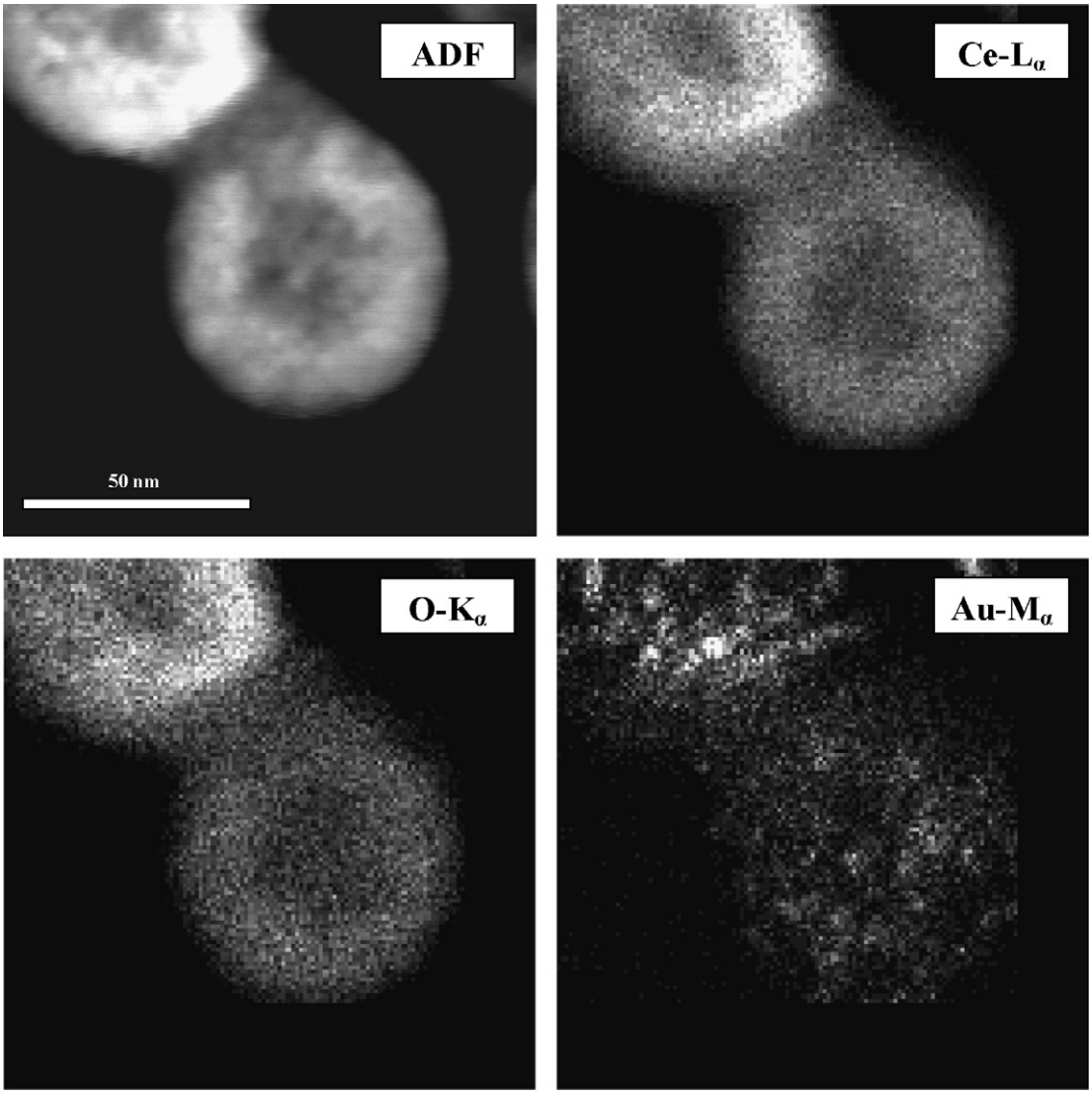

Fig. 10. Montage showing a STEM-ADF image and corresponding cerium, oxygen, and gold XEDS maps of the Au/scCeO$_2$-2 sample observed *after* catalytic testing for the CO oxidation reaction.

lar (Table 2) and similar to the particle sizes reported by Corma et al. [16]. Rather, we consider it to be due to the relative dispersion of Au on the support surfaces. In Au/unCeO$_2$, which was the poorest catalyst for CO oxidation, large (10–40 nm) Au particles were clearly resolved in the Au-M$_\alpha$ XEDS map. This is in stark contrast to Au/scCeO$_2$-2 (the best CO oxidation catalyst), for which no discrete Au particles were observed, which is consistent with the XRD pattern of this sample (Fig. 1c). Instead, the corresponding Au-M$_\alpha$ XEDS map showed the gold to be very uniformly and possibly even atomically dispersed over the entire surface of the CeO$_2$ support. This suggests that the highly dispersed Au species on CeO$_2$ are significantly more active than discrete Au nanoparticles on CeO$_2$, and that the high dispersion is enhanced by the scCO$_2$ treatment of the support. The STEM-XEDS data obtained from the catalysts displaying intermediate activity (Au/scCeO$_2$-1 and Au/scCeO$_2$-3) tend to support this correlation. The Au-M$_\alpha$ XEDS maps (Fig. 7) of these two samples show them to contain mixtures of both nanoparticulate Au (2–10 nm) and highly dispersed Au in differing proportions. The more catalytically active of these two samples (Au/scCeO$_2$-3) contains a higher fraction of highly dispersed Au species and fewer Au nanoparticles than sample Au/scCeO$_2$-1, which is marginally catalytically inferior.

We conclude that the surfaces of the supercritically prepared CeO$_2$ are able to stabilize gold, either as an atomic dispersion or as sub-1-nm clusters, and our detailed XPS studies show that the gold is present in the metallic form. It is possible that the CeO$_2$ prepared by supercritical CO$_2$ as an antisolvent may contain a high density of defects due to the rapid precipitation caused by the high supersaturation achieved with this method.

Catalyst deactivation of these dispersed Au^0 catalysts is by sintering of these small gold clusters, which can be expected under these conditions. We have previously discussed the possibility that the melting point of nanodispersed Au^0 is much lower than that of bulk gold [11] and that consequently these catalysts are difficult to stabilize under reaction conditions.

4. Conclusion

We have prepared CeO$_2$ as a support for Au nanoparticles by precipitation with scCO$_2$ as an antisolvent. Our catalytic data indicate that the activity and stability for CO oxidation of a gold catalyst supported on this material is greater than that of gold supported on regular CeO$_2$ derived from the direct calcination of Ce(acac)$_3$. We also found that these Au catalysts supported on scCeO$_2$ are among the most active catalysts yet reported for CO oxidation, considerably more active than the previously best reported catalytic activity for Au supported on CeO$_2$, and thus may have application in respiratory protection. Our studies show that this materials synthesis methodology has significant potential to produce supports that can be used to prepare highly active oxidation catalysts that can be of importance for the design of new green technologies. In particular, using scCO$_2$ in this way will permit realization of a nitrate-free route to catalytic materials, which will have an enormous positive environmental impact.

Acknowledgments

The authors acknowledge support from the EPSRC (UK), Johnson Matthey plc (ATHENA and Green Oxidation), the EU (AURICAT; contract HPRN-CT-2002-00174), the World Gold Council (GROW scheme), and Cardiff University. C.J.K. and A.A.H. gratefully acknowledge NSF funding through grants DMR-0079996, DMR-0304738, and DMR-0320906.

Supplementary material

The online version of this article contains additional supplementary material.

Please visit DOI:10.1016/j.jcat.2007.04.016.

References

[1] R.A. Sheldon, Stud. Surf. Sci. Catal. 59 (1991) 33–54.
[2] G.C. Bond, D.T. Thompson, Catal. Rev. Sci. Eng. 41 (1999) 319–388.
[3] A.S.K. Hashmi, Gold Bull. 37 (2004) 51–65.
[4] M. Haruta, Gold Bull. 37 (2004) 27–36.
[5] M. Haruta, T. Kobayashi, H. Sano, N. Yamada, Chem. Lett. 16 (1987) 405–408.
[6] P. Landon, J. Ferguson, B.E. Solsona, T. Garcia, A.F. Carley, A.A. Herzing, C.J. Kiely, S.E. Golunski, G.J. Hutchings, Chem. Commun. (2005) 3385–3387.
[7] B.T. Qiao, Y.Q. Deng, Chem. Commun. (2003) 2192–2193.
[8] A.K. Sinha, S. Seelan, S. Tsubota, M. Haruta, Angew. Chem. Int. Ed. 43 (2004) 1546–1548.
[9] A. Abad, P. Conception, A. Corma, H. Garcia, Angew. Chem. 44 (2005) 4066–4069.
[10] M.D. Hughes, Y.-J. Xu, P. Jenkins, P. McMorn, P. Landon, D.I. Enache, A.F. Carley, G.A. Attard, G.J. Hutchings, F. King, E.H. Stitt, P. Johnston, K. Griffin, C.J. Kiely, Nature 437 (2005) 1132–1135.
[11] J.K. Edwards, B.E. Solsona, P. Landon, A.F. Carley, A.A. Herzing, C.J. Kiely, G.J. Hutchings, J. Catal. 236 (2005) 69–79.
[12] D.I. Enache, J.K. Edwards, P. Landon, B.E. Solsona-Espriu, A.F. Carley, A.A. Herzing, M. Watanabe, C.J. Kiely, D.W. Knight, G.J. Hutchings, Science 311 (2006) 362–365.
[13] M.M. Schubert, S. Hackenberg, A.C. van Vee, M. Muhler, V. Plzak, R.J. Behm, J. Catal. 197 (2001) 113–122.
[14] S.K. Shakhutdinov, R. Meyer, M. Naschitzki, M. Baumer, H.-J. Freund, Catal. Lett. 86 (2003) 211–219.
[15] S. Arrii, F. Morfin, A.J. Renouprez, J.L. Rousset, J. Am. Chem. Soc. 126 (2004) 1199–1205.
[16] S. Carrettin, P. Concepcion, A. Corma, J.M. Lopez Mieto, V.F. Puntes, Angew. Chem. Int. Ed. 43 (2004) 2538–2540.
[17] J. Guzman, A. Corma, Chem. Commun. (2005) 743–745.
[18] W. Yan, S.M. Mahurin, Z.S. Pan, H. Overbury, S. Dai, J. Am. Chem. Soc. 127 (2005) 10480–10481.
[19] A.S.K. Hashmi, G.J. Hutchings, Angew. Chem. Int. Ed. 45 (2006) 7896–7936.
[20] R.M. Finch, N.A. Hodge, G.J. Hutchings, A. Meagher, Q.A. Pankhurst, M.R.H. Siddiqui, F.E. Wagner, R. Whyman, Phys. Chem. Chem. Phys. 1 (1999) 485–489.
[21] S. Golunski, R. Rajaram, N. Hodge, G.J. Hutchings, C.J. Kiely, Catal. Today 72 (2002) 107–113.
[22] M.J. Kahlich, H.A. Gasteiger, R.J. Behm, J. Catal. 182 (1999) 430–440.
[23] G. Avgouropoulos, T. Ioannides, C. Papadopoulou, J. Batista, S. Hocevar, H.K. Matralis, Catal. Today 75 (2002) 157–167.
[24] G. Avgouropoulos, T. Ioannides, H.K. Matralis, J. Batista, S. Hocevar, Catal. Lett. 73 (2001) 33–40.
[25] P. Landon, J. Ferguson, B.E. Solsona, T. Garcia, S. Al-Sayari, A.F. Carley, A.A. Herzing, C.J. Kiely, M. Makkee, J.A. Moulijn, A. Overweg,

S.E. Golunski, G.J. Hutchings, J. Mater. Chem. 16 (2006) 199–208.
[26] G.J. Hutchings, M.S. Hall, A.F. Carley, P. Landon, B.E. Solsona, C.J. Kiely, A. Herzing, M. McKee, J.A. Moulijn, A. Overweg, J.C. Fierro-Gonzalez, J. Guzman, B.C. Gates, J. Catal. 242 (2006) 71–81.
[27] M. Haruta, Catal. Surv. Jpn. 1 (1997) 61–73.
[28] M. Haruta, Osaka Kogyo Gijutsu Kenkyusho Hokoku 393 (1999) 69–71.
[29] M. Haruta, H. Kageyama, N. Kamijo, T. Kobayashi, F. Delannay, Stud. Surf. Sci. Catal. 44 (1989) 33–42.
[30] F. Moreau, G.C. Bond, A.O. Taylor, J. Catal. 231 (2005) 105–114.
[31] R. Zanella, S. Giorgio, C.R. Henry, C. Louis, J. Phys. Chem. B 106 (2002) 7634–7642.
[32] R. Zanella, L. Delannoy, C. Louis, Appl. Catal. A 291 (2005) 62–72.
[33] R. Zanella, C. Louis, Catal. Today 107–108 (2005) 768–777.
[34] W.-C. Li, M. Comotti, F. Schueth, J. Catal. 237 (2006) 190–196.
[35] M. Comotti, W.-C. Li, B. Spliethoff, F. Schueth, J. Am. Chem. Soc. 128 (2006) 917–924.
[36] J. Guzman, S. Carrettin, A. Corma, J. Am. Chem. Soc. 127 (2005) 3286–3287.
[37] H. Sakurai, T. Akita, S. Tsubota, M. Kiuchi, M. Haruta, Appl. Catal. A 291 (2005) 179–187.
[38] J. Guzman, S. Carrettin, J.C. Fierro-Gonzales, Y. Hao, B.C. Gates, A. Corma, Angew. Chem. Int. Ed. 44 (2005) 4778–4781.
[39] Q. Fu, A. Weber, M. Flytzani-Stephanopoulos, Catal. Lett. 77 (2001) 87–95.
[40] D. Andreeva, I. Ivanov, L. Ilieva, M.V. Abrashev, Appl. Catal. A 302 (2006) 127–132.
[41] P.M. Gallagher, M.P. Coffey, V.J. Krukonis, N. Klasutis, ACS Symp. Ser. (Supercrit. Fluid Sci. Technol.) 406 (1989) 334–354.
[42] D.J. Dixon, G. Luna-Bercenas, K.P. Johnston, Polymer 35 (1994) 3998–4005.
[43] A. O'Neil, C. Wilson, J.M. Webster, F.J. Allison, J.A.K. Howard, M. Poliakoff, Angew. Chem. Int. Ed. 41 (2002) 3796–3799.
[44] C.N. Field, P.A. Hamley, J.M. Webster, D.H. Gregory, J.J. Titman, M. Poliakoff, J. Am. Chem. Soc. 122 (2000) 2480–2488.
[45] E. Reverchon, G. Della Porta, D. Sannino, P. Ciambelli, Powder Technol. 102 (1999) 127–134.
[46] G.J. Hutchings, J.A. Lopez-Sanchez, J.K. Bartley, J.M. Webster, A. Burrows, C.J. Kiely, A.F. Carley, C. Rhodes, M. Hävecker, A. Knop-Gericke, R.W. Mayer, R. Schlögl, J.C. Volta, M. Poliakoff, J. Catal. 208 (2002) 197–210.
[47] For a description of Gold Reference Catalysts, see Gold Bull. 36 (2003) 1.
[48] S. Tsubota, T. Nakamura, K. Tanaka, M. Haruta, Catal. Lett. 56 (1998) 131.
[49] M. Haruta, S. Tsubota, T. Kobayashi, H. Kageyama, M.J. Genet, B. Delmon, J. Catal. 144 (1993) 175.